RSC Advances

PAPER

View Article Online
View Journal | View Issue

Cite this: *RSC Adv.*, 2022, **12**, 12871

Rapid preparation of ZnO nanocomposite hydrogels by frontal polymerization of a ternary DES and performance study

Bin Li, *[a] Mengjing Zhou, [a] Ming Cheng, [a] Jizhen Liu, [a] Xiaojia Xu[a] and Xiangyu Xie[b]

A deep eutectic solvent (DES) was synthesized from urea (U), acrylamide (AM), and choline chloride (ChCl). ZnO was dispersed in the DES as a filler, and nanocomposite hydrogels (ZnO/P(U-AM-ChCl)) were successfully prepared by frontal polymerization (FP). The hydrogels were verified by Fourier infrared spectroscopy to contain ZnO nanoparticles (ZnO-NPs). The swelling behaviour, conductivity, and antibacterial properties of the ZnO nanocomposite hydrogels were investigated. The results showed that the ZnO/P(U-AM-ChCl) hydrogels had excellent antibacterial properties and exhibited super high inhibition rates of 81.87% and 88.42% against two basic colonies of Gram-negative and Gram-positive bacteria, respectively. The equilibrium swelling of the hydrogels was found to increase significantly from 9.30 to 12.29 with the addition of ZnO, while the ZnO/P(U-AM-ChCl) hydrogel conductivity exhibited good UV sensitivity. This study provides a rapid and low-energy method for the preparation of nanocomposite hydrogels with excellent antibacterial properties.

Received 12th March 2022
Accepted 17th April 2022

DOI: 10.1039/d2ra01626e

rsc.li/rsc-advances

1 Introduction

Hydrogels are macroscopically a liquid–solid system composed of swollen solid substrates in water,[1] and microscopically a hydrophilic three-dimensional polymeric network.[2] The combination of hydrogen and ions in the three-dimensional network structure makes hydrogels insoluble in water but with good water absorption,[3] while the strength of water absorption depends on the hydrophilic functional groups in the polymer backbone.[4,5] Due to the ability of hydrogels to absorb large amounts of water, they are widely applied in several fields such as medical composites, drug transport,[6–8] wound dressings,[9] biosensors[10] and other fields.[11]

ZnO has excellent antimicrobial properties[12] and has been used in the lining of various food cans to preserve colour and prevent spoilage. Nano-ZnO possesses stronger antimicrobial properties than ZnO, which is attributed to the smaller size (less than 100 nm) and higher specific surface area, a physical property that allows it to interact more fully with bacteria and disrupt the permeability of cell membranes.[13] Compounding ZnO with hydrogels allows the hydrogels to exhibit antimicrobial properties.[14,15] Hassan *et al.*[2] prepared antimicrobial composite hydrogels with pH sensitivity by incorporating ZnO nanoparticles into dissolved starch hydrogels by *in situ* reaction, and Yadollahi *et al.*[16] achieved antimicrobial properties by generating ZnO *in situ* in dissolved carboxymethylcellulose composite hydrogels. However, these two methods have complicated preparation processes and long polymerization times, which limit the application of hydrogels.

FP is a more advanced method of polymer synthesis in which reactant monomers can be rapidly converted into polymers within a local reaction zone based on the coupling of thermal diffusion and Arrhenius reaction kinetics.[17,18] Thermal initiation is a type of FP, also known as thermal differential frontal polymerization,[19] which requires only the addition of a heat source at one end of the test tube. It is able to propagate from top to bottom by itself, thus achieving the completion of the entire polymerization. FP reduces the cost required for polymer preparation and enables high conversion rates in a shorter time.[20–22] However, the difficulty of controlling the frontal temperature, which may lead to initiator "burnout" or even monomer boiling if the frontal temperature is too high, greatly limits the application of FP.[23]

Deep eutectic solvents (DES) is a new type of ionic liquid consisting of a mixture of a hydrogen bond donor (HBD, *e.g.*, urea, acrylamide) and a hydrogen bond acceptor (HBA, *e.g.*, choline chloride). It can be adjusted for different situations to form binary, ternary, and multiple DES. The high viscosity of DES facilitates a more stable FP process. Compared to common ionic liquids, DES also has the advantages of being low-cost, easy to prepare, and recyclable.[24,25] The above properties of DES make it have a wide range of applications.[26] Based on previous studies, we developed an antimicrobial ZnO/P(U-AM-

[a]*School of Mechanical Engineering, Wuhan Polytechnic University, Wuhan, Hubei 430023, China. E-mail: lb420@whpu.edu.cn*

[b]*Hubei Key Laboratory of Theory and Application of Advanced Materials Mechanics, Wuhan University of Technology, Wuhan, Hubei 430070, China*

ChCl) nanocomposite hydrogel by adding ZnO to DES. The effect of ZnO content on the swelling properties, electrical conductivity, and antimicrobial properties of the hydrogel was investigated by dissolving ZnO in a ternary DES composed of acrylamide (AM)-choline chloride (ChCl)-urea (U). The ZnO/P(U-AM-ChCl) nanocomposite hydrogels were effectively fabricated by FP of the ZnO-dissolved DES. The structures of the nanocomposite hydrogels were characterized by scanning electron microscope (SEM) and Fourier infrared spectroscopy (FTIR) to further analyze the effect of ZnO content on the swelling properties, electrical conductivity and antibacterial properties of the composite hydrogels.

2 Experimental

2.1 Materials

N,*N*-Methylenebisacrylamide (MBA), acrylamide (AM), potassium persulfate (KPS), urea (U) and zinc oxide (ZnO) were purchased from Tianjin Comio Chemical Reagent Co. Choline chloride (ChCl) was purchased from Shanghai Shanpu Chemical Co. Before use, ChCl should be dried under vacuum at 80 °C for two hours to remove the absorbed water. The purity of all reagents is of analytical grade.

2.2 Preparation of deep eutectic solvents

The preparation of DES was carried out using the following method: ChCl as HBA, U and AM as HBD, mixed in a beaker according to the molar ratio of 1 : 1 : 1, so that the beaker was immersed in an oil bath at 80 °C (the oil surface was above the highest point of the mixed reagents) and stirred continuously using a glass rod until a clear and clarified liquid was formed. The preparation of DES is shown in Fig. 1.

2.3 Preparation of deep eutectic solvent containing ZnO

Since ZnO needs to be dissolved in DES at high temperature, while AM is prone to self-polymerization at high temperature. It is not possible to dissolve ZnO in ternary DES (T-DES) directly. To overcome the above difficulties, ChCl and U were formulated into binary DES (B-DES) according to the molar ratio of 1 : 1. After adding different mass fractions of ZnO according to the ratios, shown in Table 1, the mixture was placed in a drying oven at 100 °C until ZnO was completely dissolved. After the mixture became transparent again, AM of the same molar mass as U was added and stirred continuously at 80 °C in the environment until a clear and clarified solution was formed, and the flow chart of deep eutectic solvent preparation is shown in Fig. 2.

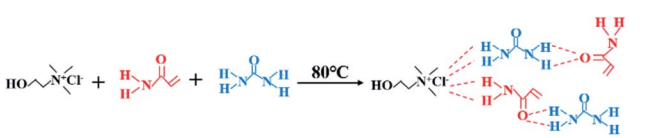

Fig. 1 Formation equation of DES.

Table 1 ZnO/P(U-AM-ChCl) nanocomposite hydrogel ratios

Sample	ZnO (wt%)	AM (g)	U (g)	KPS (wt%)	MBA (wt%)
FP0	0	2.132	1.802	0.5	1.0
FP1	0.4	2.132	1.802	0.5	1.0
FP2	0.8	2.132	1.802	0.5	1.0
FP3	1.2	2.132	1.802	0.5	1.0

Compared with our previous research,[23] the DES prepared in this paper changes the hydrogen bond donor into urea and acrylamide, and urea can form hydrogen bond with choline chloride, which wraps the ZnO-NPs formed in the process of heat treatment to prevent ZnO-NPs re-aggregation after the decrease of temperature. Because the DES prepared by urea and choline chloride can't Carry on the frontal polymerization. Therefore, acrylamide and urea are added together as hydrogen bond donors in DES, and acrylamide is reacted as a monomer in the frontal polymerization.

2.4 Frontal polymerization of deep eutectic solvents

At a constant temperature of 35 °C, 1.0 wt% MBA and 0.5 wt% KPS were added to DES according to the ratios in Table 1, followed by transferring the mixture into a glass test tube of size 100 × 12 mm, the level of the mixture was kept at 80 mm in the test tube, and a K-type thermocouple was inserted 70 mm below the liquid surface. The upper liquid surface was triggered with a soldering iron. After the formation of a stable frontal front, the iron was withdrawn and the change of frontal position with time was recorded. After the reaction, when the hydrogel cooled to room temperature, it was taken out, then cut into 1–3 mm thick discs. Finally, it was put into distilled water for a week, and then the hydrogel was freeze-dried to constant weight and set aside (Fig. 3).

2.5 Performance testing and characterization

2.5.1 SEM characterization. The specimens were taken after vacuum freeze-drying, and their cross-sections were sprayed with gold by a high vacuum ion sputtering instrument, and the cross-sectional microscopic morphology was observed by SEM.

2.5.2 FTIR characterization. The dried hydrogel fractions were ground into powder and the solid powder samples were mixed with potassium bromide, ground, and pressed for FTIR testing.

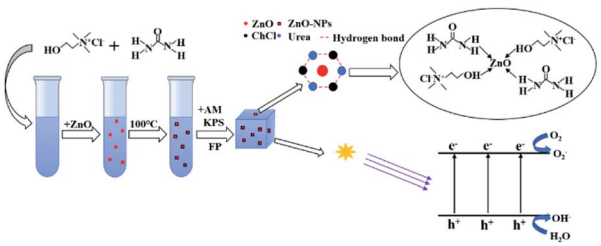

Fig. 2 Schematic diagram of preparation of ZnO nanocomposite gel.

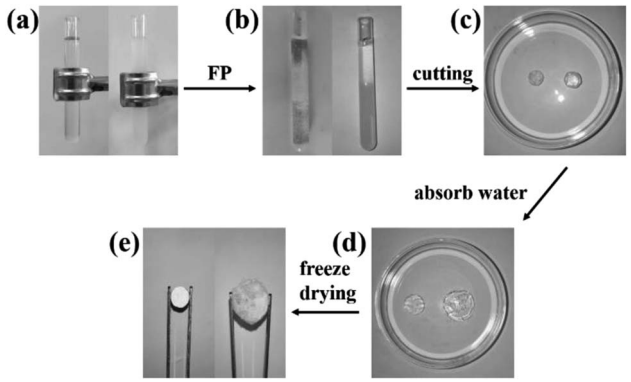

Fig. 3 (left) the picture of the hydrogel experiment without adding ZnO and (right) adding 0.4 wt% ZnO. In the figure, (a) is the mixture of the reaction, (b) the mixture that is being polymerized at the front end, (c) the hydrogel that is cut into a disk after the end of the reaction, (d) the hydrogel that absorbs water for 24 hours, and (e) the freeze-dried hydrogel.

2.5.3 Hydrogel swelling behaviour test. The disc-shaped hydrogel weighing about 50 mg was put into distilled water. The hydrogel was taken out at intervals throughout the test. The water attached on the surface of the hydrogel was blotted out with filter paper and weighed and recorded until its weight no longer changed, and then the equilibrium swelling degree (SR) of the hydrogel was calculated by eqn (1).

$$\mathrm{SR} = \frac{m_t - m_0}{m_0} \quad (1)$$

where,m_0 is the initial weight of the hydrogel,m_t is the weight of the hydrogel after the water absorption time t.

2.5.4 Hydrogel antibacterial performance test. The overnight cultures of *E. coli* and *S. aureus* were inserted into Luria–Bertani (LB) liquid medium and incubated for 2 h at 37 °C with shaking, and then 5 mL of bacterial suspension was removed and added together with hydrogels containing different mass fractions of ZnO in a triangular flask containing 70 mL of phosphate buffered salt solution (PBS). The triangular flask was placed into an environment of 37 °C for shaking incubation, and the optical density of the solution was measured at 600 nm using a digital spectrophotometer, and then the bacterial inhibition rate (BR) of the hydrogel was calculated by eqn (2).

$$\mathrm{BR} = \frac{a_0 - a_1}{a_0} \times 100\% \quad (2)$$

where a_0 is the absorbance value of the blank bacterial solution and a_1 is the absorbance value of sample bacterial solution.

2.5.5 Hydrogel conductivity testing. A cylindrical hydrogel with a radius of 5 mm and thickness of 10 mm was taken, and the resistance of the cylindrical hydrogel sample was tested by the double electrode method. And according to eqn (3), the conductivity was calculated.

$$\sigma = \frac{L}{A \times R_b} \quad (3)$$

where σ (mS m^{-1}) represents the electrical conductivity, L represents the thickness of the hydrogel, $R_b$represents the impedance, and A is the cross-sectional area of the hydrogel.

3 Results and discussion

3.1 Preparation of nanocomposite hydrogels by FP

As a filler, ZnO can inhibit the generation of bubbles and stabilize the frontal during frontal polymerization.[22] As shown in Table 2, through each parameter of the frontal polymerization, it is easy to find that with the increase of ZnO content, the polymerization temperature decreases and the reaction speed slows down. This is because that the introduction of ZnO reduces the AM of the reaction per unit volume and the double bond density, which is equivalent to the heat sink of the polymerization system.[14] As shown in Fig. 4, the displacement-time relationships of the DES system are linear, indicating that the polymerization is carried out with a constant velocity downward reaction. At the first two minutes of the polymerization reaction, the temperature in Fig. 5 is almost a constant and does not show a large increase. It then increases rapidly from room temperature to the maximum temperature of 100–130 °C during the 2–5 min time period. Combined with the above analysis, no spontaneous ontogenetic polymerization was generated during the frontal polymerization.

3.2 Infrared spectra of composite hydrogels (FTIR)

As shown in Fig. 6, the FTIR spectra of P(U-AM-ChCl) with ZnO/P(U-AM-ChCl) have a broad absorption band at 3433 cm^{-1} that is associated with the –NH asymmetric and –OH symmetric stretching vibration groups. The absorption band at 2927 cm^{-1} that is induced by the stretching vibration of the CH_3 unit, while

Table 2 Parameters of frontal polymerization

Sample	ZnO (wt%)	T_{max} (°C)	V_f (cm min^{-1})
FP0	0	123.4	2.53
FP1	0.4	118.6	1.85
FP2	0.8	115.1	1.66
FP3	1.2	101.0	1.60

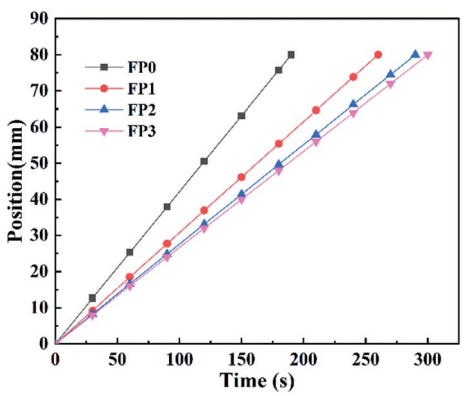

Fig. 4 Typical position–time curve during frontal polymerization.

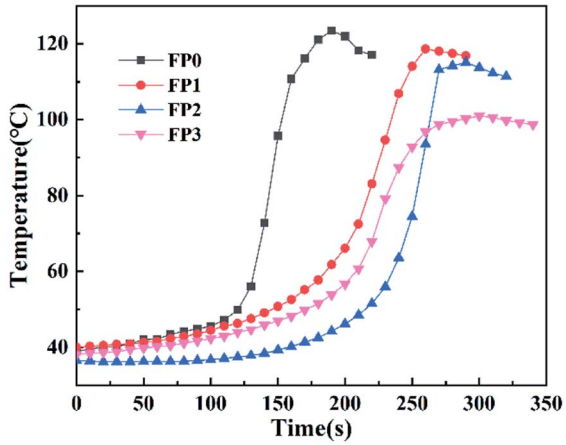

Fig. 5 Typical frontal temperature–time profile during frontal polymerization.

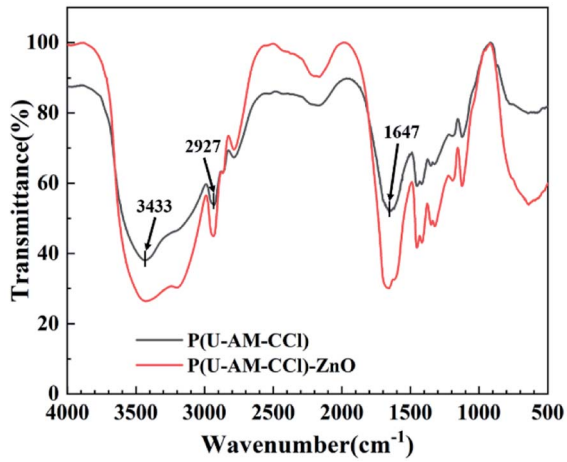

Fig. 6 FTIR spectra of P(U-AM-ChCl) and ZnO/P(U-AM-ChCl) hydrogels.

the absorption band at 1647 cm^{-1} can be attributed to the carbonyl group of P(U-AM-ChCl) hydrogel. In the P(U-AM-ChCl)-ZnO composite hydrogel, the wave number of carbonyl corresponding to the absorption band is 1664 cm^{-1}, which may be due to the combination of Zn^{2+} and urea, which makes the absorption peak shift to high frequency. And with the increase of ZnO content, the more the wave number of carbonyl group moves to high frequency.[27] The results showed that in the P(U-AM-ChCl)-ZnO composite hydrogel, these peaks shifted to 3437 cm^{-1}, 2935 cm^{-1}, indicating that the P(U-AM-ChCl) hydrogel contains ZnO nanoparticles.

3.3 Characterization of composite hydrogels

The hydrogels were soaked in deionized water for 7 days to dissolve the soluble substances, and then they were pre-frozen and freeze-dried at a temperature of −60 °C. At this time, the ice crystals filled in the pores of the hydrogel, sublimated in the freeze-dryer, resulting in the hydrogel exhibiting a uniform porous structure, as shown in Fig. 7. With the addition of ZnO,

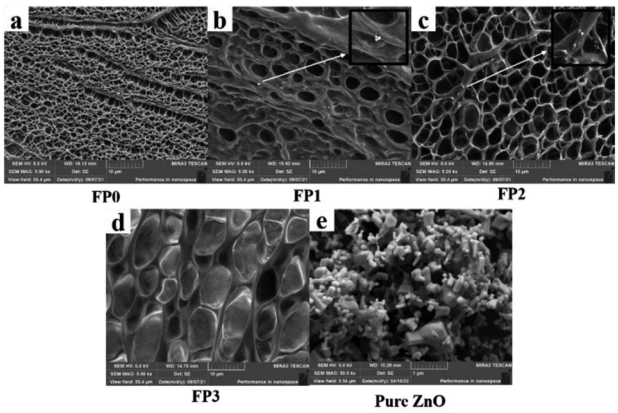

Fig. 7 SEM image of (a–d) ZnO nanocomposite hydrogel and (e) pure ZnO.

the pore size of the hydrogel cross-section increases to 10 μm which leads to a lower pore density. U in DES is a good dispersant and can bring ZnO to the dispersion level of nano-ZnO under vacuum at 100 °C, dispersing the ZnO particles in the hydrogel as ZnO-NPs.[28] As shown in Fig. 7(a), the presence of white particles was not observed in the FP0 cross section. While fine white particles can be observed in Fig. 7(b) (FP1) and Fig. 7(c) (FP2), the presence of ZnO-NPs in the hydrogel with a diameter of about 50 nm can be determined. No obvious white particles were observed in Fig. 7(d). This can be explained by the agglomeration of ZnO-NPs during the dissolution process, and the ZnO-NPs particles with increasing size are more likely to be removed during the immersion process. Fig. 7(e) is a SEM diagram of pure ZnO, from which it can be seen that the size of ZnO particles is about 200 nm. The change of ZnO size in pure ZnO and composite hydrogels proves that we have successfully prepared ZnO nanoparticles (Fig. 8).

At the same time, the composite hydrogel with 0.4 wt% ZnO content was analysed by EDX, and it was proved that the composite hydrogel contained ZnO.

3.4 Swelling behaviour of composite hydrogels

Fig. 9 shows the dissolution kinetic curves of hydrogels containing different mass fractions of ZnO. When the ZnO content in the hydrogel is 0%, 0.4%, 0.8% and 1.2%, the equilibrium swelling degree is 9.30, 11.33, 11.55 and 12.29. This is because in the process of reducing ZnO to nano-ZnO in hydrogel, the

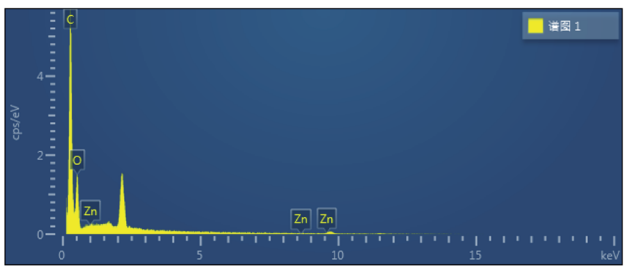

Fig. 8 EDX analysis of ZnO nanocomposite hydrogel.

hydrogel network expands moderately due to the different size of nanoparticles and the amount of surface charge, the hydrogel network expands moderately, so that the hydrogel can hold more water molecules; on the other hand, the hydrogel has a higher equilibrium swelling, which may be due to the fact that the long chains of the polymer contain a large number of hydroxyl groups, which interact with water molecules to form hydrogen bonds and thus have a higher swelling in aqueous media. In addition, the formation of ZnO-NPs in the gels by Zn^{2+} expands the gel network and improves the adsorption capacity of the hydrogel for water molecules.[29,30] Interestingly, the composite hydrogel without ZnO reached the swelling equilibrium in a short time (18 min), while the composite hydrogel without ZnO increased the swelling equilibrium time with the increase of ZnO content. With the increase of ZnO content, the equilibrium swelling time of the hydrogel was 18 minutes, 26 minutes, 33 minutes and 45 minutes, respectively. This may be due to the covalent bond between the ZnO-NPs formed by the reaction and the polymer chain, which makes the hydrogel show low adsorption, which becomes stronger with the increase of the number of ZnO-NPs.[31] Fig. 9 shows the swelling kinetic curves of hydrogels containing different mass fractions of ZnO. The swelling performance of the hydrogels increased significantly with the increase of ZnO content. When the ZnO content increased to 1.2 wt%, the increase of the swelling performance curves decreased significantly, which may be due to the addition of ZnO, which increased the cross-link density of the three-dimensional network of hydrogels. The increase of the number of cross-link sites, which shortened the chain length between the cross-link sites. The increase in the number of cross-linked sites shortens the length of the chain between the cross-linked sites and increases the elastic contraction force that hinders the swelling of the hydrogel, which reduces the network space and free water in the hydrogel, resulting in a slow increase in the SR value.[32,33]

However, when the ZnO content continues to increase to 5 wt% or 10 wt%, a large amount of ZnO reduces the crosslinking density of the hydrogel, moves the polymer chain freely, and increases the osmotic pressure inside the hydrogel. At the same time, too high content makes ZnO can't be fully heated in the process of heat treatment, resulting in the ZnO in DES can't be completely converted into ZnO-NPs. When the hydrogel is immersed in deionized water, a large number of water molecules enter the hydrogel, resulting in the collapse of the gel network inside the hydrogel, so that the hydrogel can't maintain its original shape.

3.5 Antimicrobial properties of composite hydrogels

The effect of different contents of ZnO on the antibacterial performance of *Escherichia coli* (Gram-negative bacteria) and *Staphylococcus aureus* (Gram-positive bacteria) was investigated by liquid culture method. As shown in Fig. 10, the inhibition rate of the hydrogel gradually increased with the ZnO mass fraction in the hydrogel. At a ZnO content of 1.2 wt%, the inhibition rate of the hydrogel in both colonies exceeded 80%, which is significant improvement comparing to the blank hydrogel. The main reason is that, as the mass fraction of ZnO in the hydrogel increases, the concentration of free ZnO-NPs increases during the oscillatory incubation with the bacterial suspension. More ZnO-NPs are internalized into the cells reducing the content of adenosine triphosphate and other essential energy molecules in the cells, affecting the mitochondrial function,[34] thus inhibiting energy metabolism and reducing the cell's ability to maintain normal life activities energy, the cell membrane then destabilizes and ruptures, and the cell contents leak out, which in turn makes it easy for ZnO-NPs to enter the cell.[36] As ZnO-NPs enter the cell more and accumulate inside the cell, they deplete intracellular material and interrupt DNA replication, which eventually leads to bacterial death.

In contrast, the hydrogels without ZnO addition exhibited weaker antibacterial properties, which may be the result of insufficient response to the action of KPS in the hydrogels. KPS can release highly reactive oxygen free radicals, hydroxyl free radicals, and sulfuric acid free radicals in water, which are both active components of significant microbicidal effects.[37] It can be seen in Fig. 10 that *S. aureus* is more sensitive to the changes in ZnO content in nanocomposite hydrogels relative to *E. coli*. This is because Gram-positive bacteria have only a cell wall and

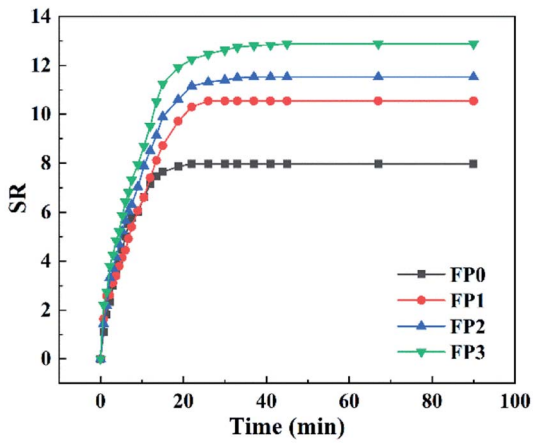

Fig. 9 Dissolution kinetic curves of ZnO nanocomposite hydrogels.

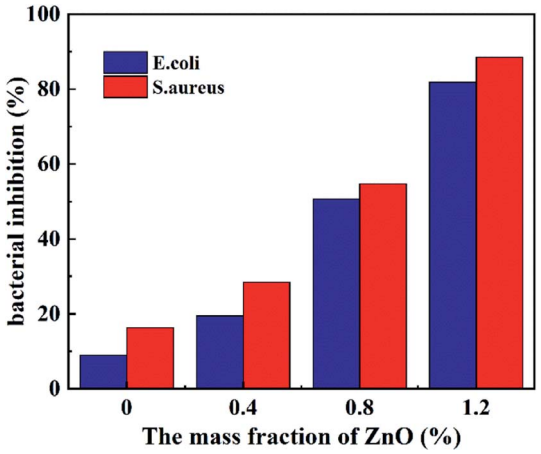

Fig. 10 Bacterial inhibition rates of ZnO nanocomposite hydrogels against *Escherichia coli* and *Staphylococcus aureus*.

plasma membrane consisting of multiple layers of peptidoglycan polymers, whereas Gram-negative bacteria possess a peptidoglycan membrane and a more complex cell wall as well as two cell membranes. The extra cellular membrane of Gram-negative bacteria affects their permeability and entry of ZnO-NPs into the cells becomes difficult, thus decreasing the cell mortality.[38,39]

Fig. 11 shows a schematic diagram of the internalization of ZnO-NPs into cells, destabilization and rupture of cell membranes, and efflux of cell contents. The entry of ZnO-NPs into cells disrupts the permeability of cell membranes, allowing large amounts of ZnO-NPs to enter the cells, while ZnO-NPs bind to intracellular components such as mimetic nuclei and ribosomes, disrupting the normal cellular machinery.[40] The consequent collapse and rupture of cell walls and outflow of cell contents eventually result in cell death. Tayel, A. *et al.* demonstrated that nano-ZnO is non-toxic to human cells and has good biocompatibility with human cells,[35] indicating that nano-ZnO composite hydrogels have promising applications in food and agriculture.

3.6 Conductivity of composite hydrogels

Fig. 12(a) represents the conductivity of ZnO/P(U-AM-ChCl) nanocomposite hydrogels added with different mass fractions of ZnO at different times. Because the composite hydrogel contains hydrophilic ChCl, which readily absorbs water molecules in air, the pore and water environment inside the hydrogel facilitates the rapid proton transfer.[41] From the swelling experiments of the hydrogels, we know that the addition of ZnO reduces the crosslinking density of the hydrogel, enhances the swelling property, and enables the hydrogel to retain more water. As seen in Fig. 12(a), the conductivity of the ZnO hydrogels increased with time, where FP3 showed a 24-fold increase to 0.116 mS m^{-1} after 24 h exposure to air. Fig. 12(b) represents the rate of change of the conductivity of the nanocomposite hydrogels under violet light irradiation at 365 nm, with the increase of ZnO content, the hydrogel's UV light sensitivity increases. When the ZnO content reaches 1.2 wt%, the conductivity of the hydrogel increases by 34.6%, which is probably because the photons of UV light are absorbed by the outer electrons of ZnO-NPs and break free from the nucleus to become free electrons, which increases the carrier

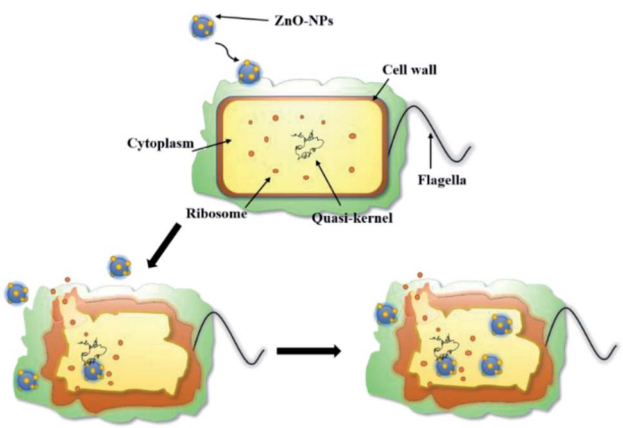

Fig. 11 Schematic diagram of the internalization of ZnO-NPs into cells to kill *E. coli*.

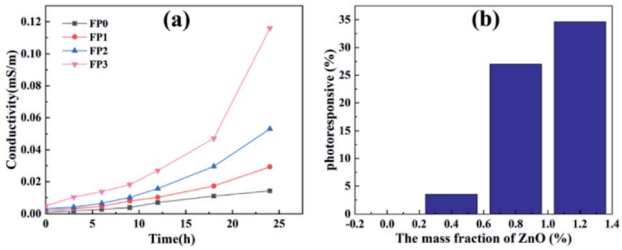

Fig. 12 (a) Electrical conductivity and (b) photosensitivity of ZnO nanocomposite hydrogels.

concentration in the hydrogel and increases the conductivity. In contrast, ZnO molecules that do not reach the nanoscale have low sensitivity to UV light irradiation,[42] which is due to the excessive particle size. The light absorption capacity is significantly enhanced only when the particle size is comparable to the light wave or even smaller, due to the size effect leading to an increase in the conduction band and valence band spacing.[43] The increasing ZnO nanoparticles promote the departure of outer electrons from the nucleus, which is the reason why ZnO/P(U-AM-ChCl) nanocomposite hydrogels are more sensitive to UV light.

4 Conclusion

In this paper, ZnO/P(U-AM-ChCl) composite hydrogel with good dispersion was prepared by frontal polymerization reaction by compounding ZnO with ChCl-U-AM ternary DES, using MBA as crosslinker and KPS as initiator, and the structure and properties of the composite hydrogel were experimentally investigated, the following conclusion can be drawn:

(1) The analysis of the swelling performance of the hydrogel showed that the swelling capacity of the hydrogel increased with the ZnO content, and the swelling performance of the hydrogel reached a maximum of 12.29 when the ZnO content reached 1.2%.

(2) Due to the semiconductor catalyst electronic structure formed by ZnO, hydrogel photosensitivity increases with ZnO content, and the photosensitivity of FP3 is nearly 10 times higher than that of FP2.

(3) The composite hydrogel shows excellent antibacterial properties. The ZnO-NPs uniformly dispersed in the hydrogel can be released to kill bacteria, and when the ZnO content is 1.2 wt%, the antibacterial rate of the hydrogel against Gram-positive and Gram-negative bacteria is up to 88.42%.

Author contributions

B. L., proposed the ideas, steps and details of the experiment, most of the experiments were done by M. J. Z., X. J. X, M. C., where M. J. Z., was instrumental in the proper conduct of the experiments and wrote the article together with B. L., and all the authors analyzed the data, discussed the conclusions.

Conflicts of interest

The authors declare that there are no competing interests regarding the publication of this article.

Acknowledgements

The work is supported by Marine Defense Technology Innovation Center Innovation Fund (JJ-2020-719-01), Natural Science Foundation of Hubei Province (2021CFB292) and Research and Innovation Initiatives of WHPU (2022J04). This work was finished at Wuhan University of Technology (WUT) and Wuhan Polytechnic University, Wuhan.

References

1 L. Toledo, L. Racine, V. Perez, J. P. Henriquez, R. Auzely-Velty and B. F. Urbano, *Mater. Sci. Eng., C*, 2018, **92**, 769–778.
2 H. Namazi, M. Hasani and M. Yadollahi, *Int. J. Biol. Macromol.*, 2019, **126**, 578–584.
3 A. S. Hoffman, *Adv. Drug Delivery Rev.*, 2012, **64**, 18–23.
4 K. Pal, A. K. Banthia and D. K. Majumdar, *Mater. Lett.*, 2008, **62**(2), 215–218.
5 M. Yadollahi, I. Gholamali, H. Namazi and M. Aghazadeh, *Int. J. Biol. Macromol.*, 2015, **73**, 109–114.
6 J. K. Jackson, K. Letchford, B. Z. Wasserman, L. Ye, W. Y. Hamad and H. M. Burt, *Int. J. Nanomed.*, 2011, **6**, 321–330.
7 M. Rasoulzadeh and H. Namazi, *Carbohydr. Polym.*, 2017, **168**, 320–326.
8 M. Yadollahi, S. Farhoudian and H. Namazi, *Int. J. Biol. Macromol.*, 2015, **79**, 37–43.
9 P. H. Corkhill, C. J. Hamilton and B. J. Tighe, *Biomaterials*, 1989, **10**(1), 3–10.
10 G. P. Andreas Richter, K. Stephan, L. Jens, A. Karl-Friedrich and P. A. Hans-Jürgen, *Sensors*, 2008, 561–581.
11 Y. Jiang, S. Li, Y. Chen, S. Yan, M. Tao and P. Wen, *Ind. Eng. Chem. Res.*, 2020, **59**(4), 1526–1533.
12 L. Zhang, Y. Ding, M. Povey and D. York, *Prog. Nat. Sci.*, 2008, **18**(8), 939–944.
13 Y. Xie, Y. He, P. L. Irwin, T. Jin and X. Shi, *Appl. Environ. Microbiol.*, 2011, **77**(7), 2325–2331.
14 D. I. Fortenberry and J. A. Pojman, *J. Polym. Sci., Part A: Polym. Chem.*, 2000, **38**(7), 1129–1135.
15 V. B. Schwartz, F. Thétiot, S. Ritz, S. Pütz, L. Choritz, A. Lappas, R. Förch, K. Landfester and U. Jonas, *Adv. Funct. Mater.*, 2012, **22**(11), 2376–2386.
16 M. Yadollahi, I. Gholamali, H. Namazi and M. Aghazadeh, *Int. J. Biol. Macromol.*, 2015, **74**, 136–141.
17 J. A. Pojman, J. Willis, D. Fortenberry, V. Ilyashenko and A. M. Khan, *J. Polym. Sci., Part A: Polym. Chem.*, 1995, **33**(4), 643–652.
18 J. A. Pojman, G. Curtis and V. M. Ilyashenko, *J. Am. Chem. Soc.*, 1996, **118**(15), 3783–3784.
19 J. A. Pojman, *Nonlinear Dynamics with Polymers*, 2010.
20 J. D. Mota-Morales, M. C. Gutierrez, I. C. Sanchez, G. Luna-Barcenas and F. del Monte, *Chem. Commun.*, 2011, **47**(18), 5328–5330.
21 K. F. Fazende, M. Phachansitthi, J. D. Mota-Morales and J. A. Pojman, *J. Polym. Sci., Part A: Polym. Chem.*, 2017, **55**(24), 4046–4050.
22 L. Chen, T. Hu, H. Yu, S. Chen and J. A. Pojman, *J. Polym. Sci., Part A: Polym. Chem.*, 2007, **45**(18), 4322–4330.
23 B. Li, J. Liu, D. Fu, Y. Li, X. Xu and M. Cheng, *RSC Adv.*, 2021, **11**(56), 35268–35273.
24 Q. Zhang, K. De Oliveira Vigier, S. Royer and F. Jerome, *Chem. Soc. Rev.*, 2012, **41**(21), 7108–7146.
25 E. L. Smith, A. P. Abbott and K. S. Ryder, *Chem. Rev.*, 2014, **114**(21), 11060–11082.
26 J. D. Mota-Morales, M. C. Gutiérrez, M. L. Ferrer, I. C. Sanchez, E. A. Elizalde-Peña, J. A. Pojman, F. D. Monte and G. Luna-Bárcenas, *J. Polym. Sci., Part A: Polym. Chem.*, 2013, **51**(8), 1767–1773.
27 J. Wang, Q. Li, M. M. Li, T. H. Chen, Y. F. Zhou and Z. B. Yue, *Bioresour. Technol.*, 2014, **163**, 374–376.
28 L. Cheng, L. Zheng, G. Li, Q. Yin and K. Jiang, *Nanotechnology*, 2008, **19**(7), 075605.
29 T. Jayaramudu, G. M. Raghavendra, K. Varaprasad, R. Sadiku, K. Ramam and K. M. Raju, *Carbohydr. Polym.*, 2013, **95**(1), 188–194.
30 T. Jayaramudu, G. M. Raghavendra, K. Varaprasad, R. Sadiku and K. M. Raju, *Carbohydr. Polym.*, 2013, **92**(2), 2193–2200.
31 S. Sattari, A. Dadkhah Tehrani and M. Adeli, *Polymers*, 2018, **10**, 6.
32 Z. Jovanovic, A. Krkljes, J. Stojkovska, S. Tomic, B. Obradovic, V. Miskovic-Stankovic and Z. Kacarevic-Popovic, *Radiat. Phys. Chem.*, 2011, **80**(11), 1208–1215.
33 Y. L. Luo, C. H. Zhang, Y. S. Chen and W. Yang, *Mater. Res. Innovations*, 2013, **13**(1), 18–27.
34 H. Chi, Y. Qiao, B. Wang, Y. Hou, Q. Li, K. Li and Z. Liu, Swelling, thermal stability, antibacterial properties enhancement on composite hydrogel synthesized by chitosan-acrylic acid and ZnO nanowires, *Polym.-Plast. Technol. Mater.*, 2019, **58**(15), 1649–1661.
35 A. A. Tayel, W. F. El-Tras, S. Moussa, A. F. El-Baz, H. Mahrous, M. F. Salem and L. Brimer, *J. Food Saf.*, 2011, **31**(2), 211–218.
36 A. Jain, R. Bhargava and P. Poddar, *Mater. Sci. Eng., C*, 2013, **33**(3), 1247–1253.
37 G. Ghanizadeh, A. N. Ara, D. Esmaili and H. J. Masoumbeigi, *Iran. J. Public Health*, 2015, **44**(10), 1376.
38 G. Fu, P. S. Vary and C.-T. J. Lin, *J. Phys. Chem. B*, 2005, **109**(18), 8889–8898.
39 K. H. Tam, A. B. Djurišić, C. M. N. Chan, Y. Y. Xi, C. W. Tse, Y. H. Leung, W. K. Chan, F. C. C. Leung and D. W. T. Au, *Thin Solid Films*, 2008, **516**(18), 6167–6174.
40 Z. Cao, Y. Luo, Z. Li, L. Tan, X. Liu, C. Li, Y. Zheng, Z. Cui, K. W. K. Yeung, Y. Liang, S. Zhu and S. Wu, *Macromol. Biosci.*, 2021, **21**(1), e2000252.
41 H. Ding, X. Liang, Q. Wang, M. Wang, Z. Li and G. Sun, *Carbohydr. Polym.*, 2020, **248**, 116797.
42 M. Ghosh, R. S. Ningthoujam, R. K. Vatsa, D. Das, V. Nataraju, S. C. Gadkari, S. K. Gupta and D. Bahadur, *J. Appl. Phys.*, 2011, **110**, 5.
43 H. K. Verma, D. Rehani, S. N. Sharma and K. K. Maurya, *Optik*, 2020, **204**, 154–164.